BOLETIN DE LOS OBSERVATORIOS DE TONANTZINTLA Y TACUBAYA, Nº 37, 6, 1971.

EVOLUTION OF STELLAR MODELS WITH HIGH METAL CONTENT

Silvia Torres-Peimbert

SUMARIO

Se presentan modelos evolutivos para masas de 1 a 1.45 $M_\odot$ y composiciones químicas comprendidas de $Z = 0.023$ a 0.10 y $X = 0.60$ a 0.68. Estas secuencias fueron calculadas con el programa de evolución estelar de Berkeley. Se estudia en detalle el efecto que tiene la abundancia de metales en la estructura y evolución de modelos de 1.25 $M_\odot$. Se encuentra que para las composiciones químicas consideradas la presencia del núcleo convectivo durante la combustión de hidrógeno en el centro depende únicamente de la luminosidad de los modelos en dicha secuencia. No se presentan núcleos convectivos en modelos de la secuencia principal más débiles que $M_{bol} = 4.6$. La edad máxima para este fenómeno es de 4.2×10^9 años. Este resultado implica que cualquier cúmulo galáctico que presente discontinuidad sobre la secuencia principal es más joven que esta edad límite.

ABSTRACT

Evolutionary sequences for stellar configurations between 1 and 1.45 $M_\odot$ with chemical abundances varying from $Z = 0.023$ to 0.10 and from $X = 0.60$ to 0.68 were computed using the Berkeley Stellar Evolution program. The effect of high metal abundances on the structure and evolution of models of 1.25 $M_\odot$ is studied in detail. It is found that for the compositions under consideration, the presence of a hydrogen-burning convective core is directly determined by the luminosity of the models on the main sequence. No core is present for an age zero main sequence model fainter than $M_{bol} = 4.6$ and the maximum age for a model with a core is 4.2×10^9 years; this result implies that any cluster with an observed gap is younger than this age.

I. Introduction

The effects on the main sequence of variations in chemical abundance for population I models are well known: for a given mass, increasing Z or X lowers the luminosity and surface temperature (Schwarzchild 1958). Computations by several investigators have confirmed the predicted changes for the range $0.01 \leq Z \leq 0.03$ (cf. Iben 1963; Demarque and Larson 1964; Pearce and Bahng 1965).

At present there is evidence that our galaxy contains objects with photospheric metal abundances higher than the Hyades. Among the Super-metal-rich objects there are G and K dwarfs (van den Bergh and Sackmann 1965; Pagel 1966; Taylor 1967, 1970; Greenstein and Oinas 1968; Spinrad and Luebke 1970), field K giants and subgiants (Spinrad and Taylor 1969), the main sequence and K giant stars of open clusters like M67 and NGC 188 (Spinrad, Greenstein, Taylor and King 1970; Spinrad and Taylor 1967), and the K giants of NGC 6791 (Spinrad and Taylor 1971*a*). Also it has been found that the nuclei of some massive galaxies like M31 and M81 contain a substantial number of SMR stars (Spinrad and Peimbert 1972; Spinrad and Taylor 1971*b*). Some of these objects have a metal to hydrogen abundance ratio as large as 4 times the solar value.

It is thus necessary to investigate in detail the evolution of configurations with metal abundance in excess of normal population I abundances. Already some evolutionary computations of models with large Z have been carried out. Demarque and Schlesinger (1969) have computed homogeneous models for a wide range of chemical compositions $0.01 \leq Z \leq 0.10$ and $0.37 \leq X \leq 0.67$ for masses close to 1 $M_\odot$ and have compared the theoretical main sequences with the observations. Aizenman, Demarque, and Miller (1969) have constructed evolutionary models with $Z = 0.03$ and $Z = 0.06$ varying the stellar masses and helium abundances such that the main sequence is at the same luminosity and have compared their results to the observed gap of the H-R diagram of M67 and NGC 188. Demarque and Heasley (1971) have advanced the evolutionary models by Aizenman *et al.* to the base of the Hayashi tracks to compare with the maximum observed luminosity above the gap on the extended main sequence.

The purpose of this paper is to report computations of evolutionary sequences of configurations of masses $1.0\ M_\odot \leq M \leq 1.45\ M_\odot$ of metal abundances in the range $0.023 \leq Z \leq 0.10$, in order to have material available to compare with "super-metal-rich" stars and clusters. The evolutionary characteristics of models of 1.25 $M_\odot$ are presented in more detail. Based on these computations Torres-Peimbert (1969, 1971) has derived the age of the SMR galactic clusters, NGC 188 and NGC 6791 and Torres-Peimbert and Spinrad (1971) have determined the age of some individual SMR stars.

Section II contains a description of the method of computation, section III the mass and composition of the model sequences and sections IV to VII the detailed comparison of the phases of evolution for the configurations of 1.25 $M_\odot$; a discussion is presented in section VIII.

II. Method of Computation

For the present investigation the Berkeley evolutionary program was used. The general outline of the method used here has been described by Henyey, Forbes, and Gould (1964); the equation of state by Bodenheimer, Forbes, Gould, and Henyey (1965); and the atmosphere calculation by Henyey, Vardya, and Bodenheimer (1965), as modified by a scaled T-τ relation found from limb darkening studies of the sun discussed by K. S. Krishna Swamy (1966, 1968). The numerical treatment of the nuclear reactions for hydrogen burning and their effect on chemical composition used was given by Bodenheimer *et al.* (1965); the values for the thermonuclear cross sections have been taken from Reeves (1965). The radiative opacities used are interpolations from the tables of Cox (1965), Cox and Stewart (1965, 1968) and Cox, Stewart, and Eilers (1965). The interpolations can reproduce the original tables with a mean deviation of 3% while allowing for varying chemical composition. Comparison with more recent tables (Cox and Stewart 1970) yields a mean deviation of 4% over the range of temperatures, densities, and compositions available. However, the values for the opacities used are substantially lower (from 30% to 50%) than the opacities that include autoionization (Watson 1970). The electron conduction opacity program used has been described by Hubbard and Lampe (1969).

III. Evolutionary Models

The evolution of configurations of masses ranging from 1.0 to 1.45 $M_\odot$, and metal contents from 0.023 to 0.10 by mass, were computed. The masses and initial compositions of these configurations are listed in Table 1. The ratio of He to H is constant for models *A* to *H*.

TABLE 1

Mass and Chemical Composition of the Computed Evolutionary Models

Model	*Mass* ($M_\odot$)	*X*	*Z*	*Model*	*Mass* ($M_\odot$)	*X*	*Z*
A	1.0	0.60	0.10	*F*	1.25	0.633	0.05
B	1.25	0.60	0.10	*G*	1.0	0.651	0.023
C	1.35	0.60	0.10	*H*	1.25	0.651	0.023
D	1.45	0.60	0.10	*I*	1.25	0.682	0.10
E	1.0	0.633	0.05				

The relative abundances among the heavy elements used for the computations are those obtained spectroscopically by Goldberg, Müller, and Aller (1960) for the photosphere of the sun. The abundance of neon used for these calculations, as being representative of population I stars, was $N(\mathrm{Ne})/N(\mathrm{C} + \mathrm{N} + \mathrm{O}) = 0.34$, taken from the spectroscopic determinations of O and B stars as summarized by Aller (1961). The initial relative breakdown of the heavy elements by mass is given in Table 2, where elements heavier than neon include Na, Mg, Al, Si, S, Ca, Fe, and Ni. The species heavier than Ne are needed to describe physical conditions in the stellar atmosphere. Not all elements are represented in the table, the choice of elements represents a compromise which attempts to describe ionization properties of the heavy elements in an average way.

TABLE 2

Relative Abundances by Weight of the Heavy Elements

Atomic Number	*Weight*	*Atomic Number*	*Weight*
12	0.177	16	0.414
13	0.002	20	0.300
14	0.0331	>20	0.0739

The ratio of mixing length to pressure scale height used in the computations was $l/H = 1.50$.

IV. Pre-Main Sequence Evolution

Two of our evolutionary sequences (Models *C* and *H*) were started at the convective contraction phase from a mass distribution corresponding to a polytrope of index 1.5. These models developed a radiative core and proceeded their evolution contracting, while the radiative core continued to grow monotonically with time. The rest of the models were started already along the radiative contraction phase with the convective envelope including only 17% of the total mass, from a mass distribution copied from Model *C*.

Since the breakdown of the heavy elements in the initial composition differs from CNO equilibrium abundances, all sequences developed a transient convective core associated with achieving equilibrium concentrations of the CNO elements on their approach to the main sequence.

All the pre-main sequence tracks of the models under consideration exhibit essentially the same characteristics. Along the radiative contraction phase both effective temperature and luminosity increase steadily, since the flux of energy in most of the star is controlled by a decreasing opacity with rising interior temperature, until the increase in luminosity and temperature is stopped soon after the C^{12} burning core starts to develop. A decrease in both luminosity and effective temperature takes place while the core attains its largest size and starts to recede; the models later resume their increase in luminosity and surface temperature at a much lower rate.

Listed in Table 3 are the surface and central characteristics of the models as well as the relative masses of the convective core and convective envelope during selected evolutive phases. Namely: point 0 corresponds to the onset of C^{12} burning; point 1, to the minimum luminosity; point 2, to the disappearance or minimum size of the convective core; point 3, to the beginning of the main sequence defined as the stage where the luminosity contributed by nuclear transformation is 99.8% of the total luminosity. The rest of the selected points will be described in §V. Time zero was identified with the onset of the main sequence since it is uncertain at what time a real star first reaches its Hayashi track after dynamic collapse (Upton, Little and Dworetsky 1968).

The transition from predominantly gravitational energy production to predominantly nuclear energy production is presented in detail in Figure 1 for the four configurations of mass 1.25 $M_\odot$. These figures exhibit the time behavior of: bolometric magnitude, central temperature, central density, fractional mass of the convective core, relative abundances of central carbon and nitrogen, and the ratio of nuclear production to total luminosity.

From Figure 1 it can be seen that along the radiative contraction phase the evolutionary configurations become more centrally condensed, with increasing central temperatures and densities until the C^{12} begins to burn rapidly near the center, when the trapped thermal energy builds up a small convective core that grows rapidly with the corresponding decrease in the density and temperature gradients; that is, the central regions expand with subsequent cooling unitl the C^{12} burning core is fully developed, then gradual contraction and heating of the core resumes throughout the C^{12} burning stage. When equilibrium abundances of C^{12} and N^{14} at the center have essentially been reached, the core disappears. The total mass of N^{14} exceeds the initial mass of both carbon and nitrogen after equilibrium has been attained, since through the $C^{12}(p, \gamma)\, N^{13}(e^+ \nu)\, C^{13}(p, \gamma)\, N^{14}$ reactions part of the initial hydrogen contributes 2/12ths of the mass of each nucleus of C^{12} to make a nucleus of N^{14}. At the onset of the main sequence the ratio $N(C^{12})/N(N^{14})$ at the centers of Model *B* and Model *H* are 6.5×10^{-3} and 7.3×10^{-3}, which are equilibrium ratios for temperatures of 1.65×10^7 and 1.8×10^7°K, respectively (Caughlan and Fowler 1962).

It is of interest to analyze whether the behavior of configurations with different chemical abundances follow the predictions that can be made from very rough approximations. Assuming that during the pre-main sequence carbon burning phase the stars are homogeneous configurations; that the equation for the ideal gas is valid, $p = \frac{1}{\mu}\frac{k}{H}\varrho T$; that the opacity law throughout the star is of the type $\varkappa = \varkappa_0 \varrho T^{-3.5}$; and that the interpolation formula for the generation of energy, $\varepsilon = \varepsilon_0 \varrho T^\nu$, can be used; then the mass and chemical composition dependence of the luminosity can be expressed as

$$L \propto \frac{\mu^{7.5} M^{5.5}}{\varkappa_0} \left[\frac{\mu^{7.5-\nu} M^{3.5-\nu}}{\varkappa_0 \varepsilon_0}\right]^{\frac{1}{2\nu+5}}. \qquad (1)$$

In the case of stars of the same mass where the opacity is mainly due to bound-free absorption, $\varkappa_0 \propto Z(1 + X)$; and the energy is generated by the CNO cycle, $\varepsilon_0 \propto ZX$, and $\nu \sim 20$; the dependence of the luminosity on chemical abundance can be expressed as

$$L \propto \frac{\mu^{7.22}}{[Z(1 + X)]^{1.02}\,(ZX)^{0.02}}. \qquad (2)$$

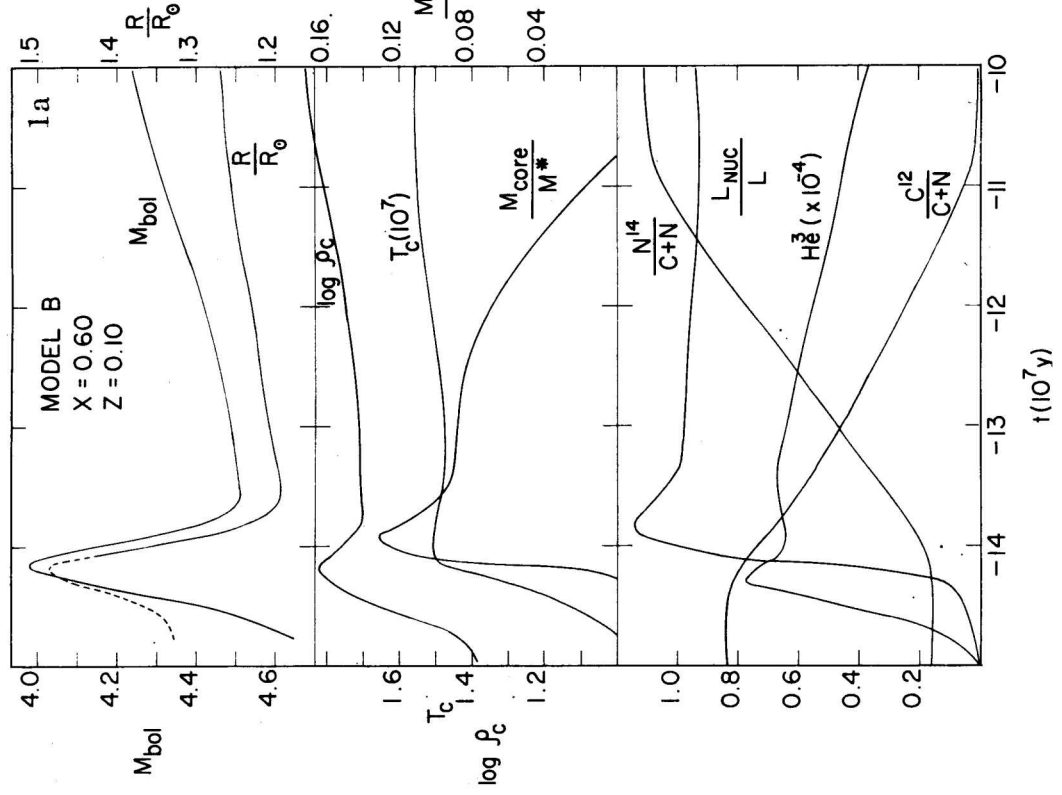

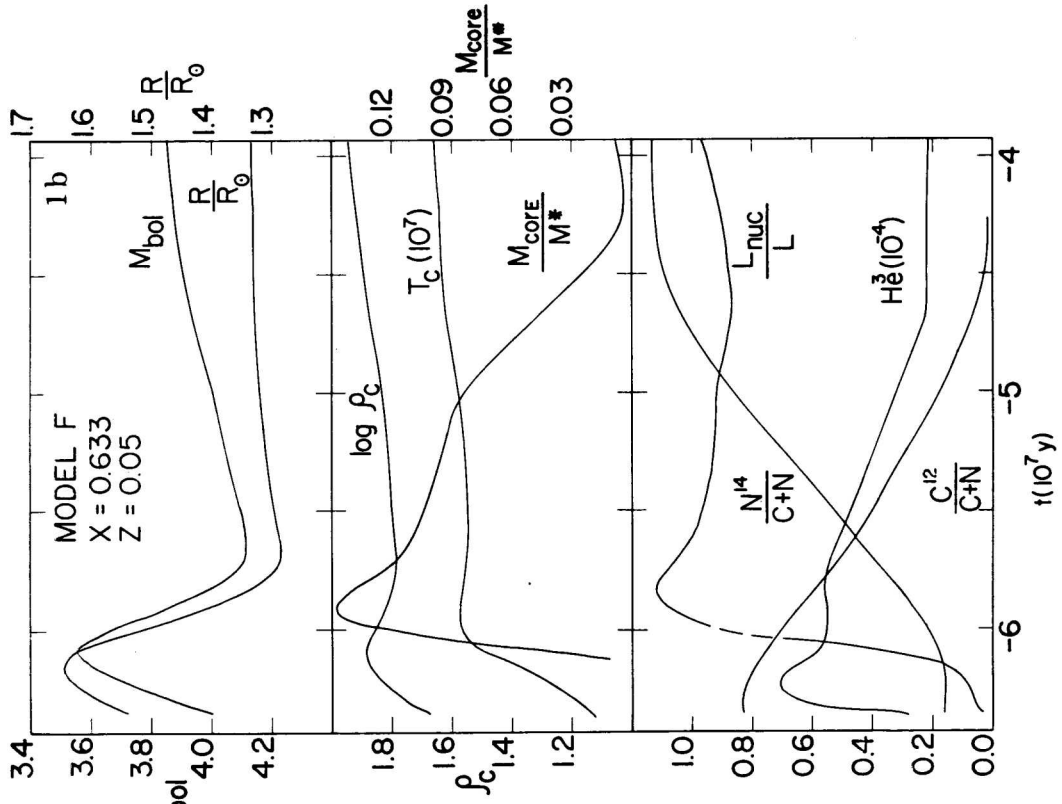

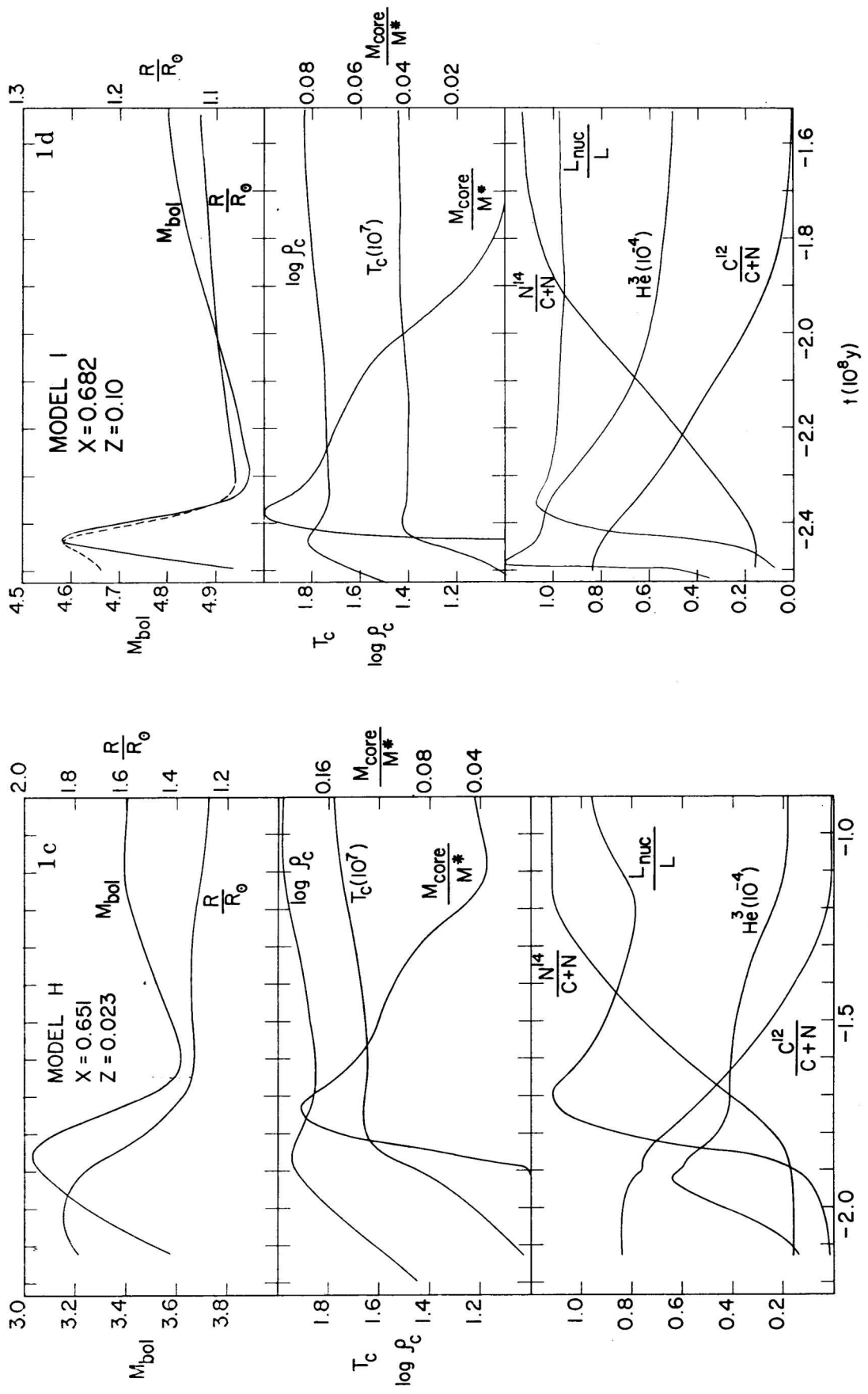

Fig. 1.—*Time variation of characteristics of pre-main sequence evolution for models of 1.25 $M_\odot$. Top section shows total radius and bolometric magnitude; middle section depicts the fraction of the mass of the convective core, central temperature and density; bottom section exhibits the ratio of nuclear luminosity for the whole star, the mass ratio of N^{14} and C^{12} to total carbon and nitrogen in the center, and the abundance by mass of He^3 in the center.*

TABLE 3

Evolutionary Tracks

	Age	M_{bol}	log T_e	$R/R_\odot$	T_c	ρ_c	X_c	m_c/m_*	m_e/m_*
			MODEL A	M=1 $M_\odot$	X=0.60, Z=0.10				
0	-3.124(8)	5.152	3.7268	0.993	1.323(7)	7.703(1)	0.600	0.031	0.051
1	-2.954(8)	5.485	3.7194	0.881	1.376(7)	6.497(1)	0.599	0.074	0.055
2	-2.318(8)	5.390	3.7256	0.895	1.394(7)	7.496(1)	0.594	0.000	0.047
3	0.000	5.293	3.7318	0.909	1.421(7)	8.827(1)	0.580	-	0.038
	2.887(9)	5.089	3.7367	0.976	1.570(7)	1.306(2)	0.324	-	0.033
4	5.032(9)	4.955	3.7367	1.039	1.710(7)	2.069(2)	0.070	-	0.035
	8.123(9)	4.638	3.7341	1.216	1.807(7)	4.752(2)	0.000	-	0.041
	9.873(9)	4.341	3.7230	1.467	1.872(7)	1.871(3)	-	-	0.073
7	1.036(10)	4.302	3.7001	1.661	2.152(7)	8.508(3)	-	-	0.208
8	1.103(10)	2.962	3.6653	3.613	2.634(7)	6.713(4)	-	-	0.756
			MODEL B	M=1.25 $M_\odot$	X=0.60, Z=0.10				
0	-1.421(8)	4.018	3.7534	1.481	1.389(7)	6.583(1)	0.600	0.013	0.011
1	-1.358(8)	4.513	3.7505	1.195	1.485(7)	5.034(1)	0.599	0.099	0.019
2	-1.073(8)	4.295	3.7615	1.255	1.556(7)	6.650(1)	0.595	0.000	0.007
3	0	4.163	3.7714	1.275	1.666(7)	8.075(1)	0.582	0.028	0.003
	1.344(9)	4.075	3.7654	1.364	1.790(7)	9.705(1)	0.368	0.045	0.004
4	2.423(9)	4.038	3.7560	1.450	1.981(7)	1.447(2)	0.081	0.033	0.009
5	2.792(9)	3.817	3.7622	1.560	1.916(7)	3.192(2)	0.001	0.000	0.004
6	4.275(9)	3.483	3.7362	2.050	2.001(7)	2.392(2)	0.000	-	0.027
7	4.488(9)	3.677	3.7014	2.201	2.684(7)	1.647(4)	-	-	0.239
	4.922(9)	1.656	3.6514	7.029	3.177(7)	1.129(5)	-	-	0.807
8	5.014(9)	-0.510	3.5926	24.98	4.507(7)	2.316(5)	-	-	0.765
			MODEL C	M=1.35 $M_\odot$	X=0.60, Z=0.10				
0	-1.004(8)	3.627	3.7608	1.714	1.411(7)	6.094(1)	0.600	0.009	0.003
1	-9.550(7)	4.173	3.7595	1.340	1.519(7)	4.572(1)	0.599	0.103	0.009
2	-6.945(7)	3.865	3.7767	1.427	1.611(7)	6.898(1)	0.595	0.000	0.001
3	0.000	3.796	3.7845	1.421	1.729(7)	7.500(1)	0.584	0.043	0.000
	6.285(8)	3.755	3.7803	1.477	1.800(7)	8.126(1)	0.461	0.057	0.000
4	1.811(9)	3.722	3.7637	1.618	1.994(7)	1.202(2)	0.111	0.040	0.003
5	2.168(9)	3.472	3.7717	1.750	1.976(7)	2.975(2)	0.001	0.000	0.001
	2.925(9)	3.245	3.7590	2.060	1.926(7)	7.479(2)	0.000	-	0.002

TABLE 3 (continued)

	Age	M_{bol}	log T_e	$R/_R$	T_c	ρ_c	X_c	m_c/m_*	m_e/m_*
			MODEL D	M=1.45 $M_\odot$	X=0.60, Z=0.10				
0	-6.137(7)	3.273	3.7711	1.923	1.491(7)	5.199(1)	0.600	0.070	0.001
1	-5.711(7)	3.848	3.7673	1.501	1.547(7)	4.182(1)	0.599	0.103	0.003
2	-3.703(7)	3.499	3.7905	1.585	1.663(7)	6.631(1)	0.595	0.000	0.000
3	0	3.457	3.7985	1.559	1.779(7)	6.946(1)	0.589	0.050	-
	3.148(8)	3.439	3.7953	1.593	1.826(7)	7.156(1)	0.518	0.069	0.000
4	1.623(9)	3.383	3.7694	1.843	2.116(7)	1.247(2)	0.531	0.037	0.001
5	1.847(9)	3.091	3.7819	1.989	1.998(7)	3.483(2)	0.000	0.000	0.000
6	2.437(9)	2.864	3.7559	2.489	2.015(7)	1.542(3)	-	-	0.001
7	2.618(9)	3.262	3.7020	2.658	3.160(7)	2.149(4)	-	-	0.250
	2.905(9)	1.197	3.6480	8.820	3.429(7)	1.306(5)	-	-	0.827
8	2.914(9)	1.056	3.6443	9.572	3.512(7)	1.377(5)	-	-	0.826
			MODEL E	M=1 $M_\odot$	X=0.633, Z=0.05				
0	-1.563(8)	4.750	3.7492	1.078	1.385(7)	8.899(1)	0.633	0.055	0.020
1	-1.447(8)	5.124	3.7437	0.931	1.421(7)	7.815(1)	0.632	0.083	0.024
2	-9.976(7)	5.016	3.7498	0.951	1.442(7)	9.194(1)	0.629	0.000	0.018
3	0	4.979	3.7522	0.957	1.460(7)	9.733(1)	0.620	-	0.016
	2.315(9)	4.773	3.7553	1.037	1.604(7)	1.423(2)	0.358	-	0.014
4	4.212(9)	4.612	3.7540	1.124	1.777(7)	2.384(2)	0.070	-	0.015
	7.765(9)	4.057	3.7395	1.551	1.930(7)	1.361(3)	0.000	-	0.031
			MODEL F	M=1.25 $M_\odot$	X=0.633, Z=0.05				
0	-6.126(2)	3.579	3.7751	1.640	1.430(7)	7.702(1)	0.633	0.013	0.001
1	-5.613(7)	4.116	3.7741	1.286	1.545(7)	6.144(1)	0.633	0.110	0.002
2	-4.263(7)	3.879	3.7904	1.331	1.639(7)	8.314(1)	0.630	0.005	0.000
3	0	3.841	3.7970	1.314	1.710(7)	9.023(1)	0.624	0.038	0.000
	7.768(8)	3.756	3.7936	1.388	1.802(7)	1.020(2)	0.479	0.054	0.000
4	2.171(9)	3.666	3.7736	1.587	2.091(7)	1.716(2)	0.065	0.040	0.001
5	2.376(9)	3.422	3.7858	1.678	1.973(7)	4.369(2)	0.001	0.000	0.000
6	3.408(9)	3.127	3.7537	2.229	2.047(7)	2.222(3)	0.000	-	0.004

TABLE 3 (continued)

	Age	M_{bol}	log T_e	$R/_R$	T_c	ρ_c	X_c	m_c/m_*	m_e/m_*
			MODEL G	M=1 $M_\odot$	X=0.651, Z=0.023				
0	-6.316(7)	4.158	3.7770	1.245	1.414(7)	1.013(2)	0.651	0.034	0.001
1	-5.549(7)	4.641	3.7755	1.004	1.499(7)	8.981(1)	0.650	0.104	0.003
2	-2.784(7)	4.536	3.7830	1.018	1.540(7)	1.051(2)	0.647	0.012	0.001
3	0	4.529	3.7835	1.019	1.547(7)	1.064(2)	0.644	0.015	0.001
	2.824(8)	4.497	3.7840	1.031	1.564(7)	1.104(2)	0.620	0.017	0.001
	1.458(9)	4.346	3.7857	1.097	1.677(7)	1.405(2)	0.443	0.011	0.001
4	3.239(9)	4.122	3.7821	1.237	1.970(7)	2.660(2)	0.059	0.006	0.001
5	3.537(9)	4.068	3.7825	1.265	1.948(7)	3.272(2)	0.020	0.000	0.001
6	5.689(9)	3.448	3.7429	2.020	2.139(7)	4.536(3)	0.000	-	0.017
			MODEL H	M=1.25 $M_\odot$	X=0.651, Z=0.023				
0	-1.886(7)	3.059	3.8139	1.743	1.463(7)	8.460(1)	0.651	0.004	0.000
1	-1.573(7)	3.617	3.8163	1.333	1.640(7)	7.168(1)	0.650	0.134	-
2	-1.043(7)	3.393	3.8460	1.289	1.756(7)	9.597(1)	0.649	0.035	-
3	0	3.430	3.8492	1.249	1.794(7)	9.833(1)	0.647	0.063	-
	5.605(8)	3.334	3.8451	1.330	1.876(7)	1.084(2)	0.521	0.078	-
	1.277(9)	3.230	3.8261	1.523	2.005(7)	1.292(2)	0.298	0.073	-
4	1.817(9)	3.162	3.8040	1.740	2.229(7)	1.806(2)	0.062	0.056	-
5	1.926(9)	2.887	3.8373	1.694	2.170(7)	5.721(2)	0.000	0.000	-
6	2.508(9)	2.567	3.7752	2.612	2.236(7)	3.862(3)	-	-	0.000
7	2.636(9)	2.964	3.7070	2.979	3.130(7)	2.772(4)	-	-	0.225
	2.904(9)	0.926	3.6576	9.562	3.513(7)	1.375(5)	-	-	0.780
8	2.923(9)	0.505	3.6493	12.06	3.771(7)	1.606(5)	-	-	0.775
			MODEL I	M=1.25 $M_\odot$	X=0.682, Z=0.10				
0	-2.428(8)	4.583	3.7329	1.255	1.361(7)	6.561(1)	0.682	0.033	0.029
1	-2.278(8)	4.790	3.7266	1.081	1.406(7)	5.408(1)	0.681	0.078	0.032
2	-1.698(8)	4.825	3.7350	1.111	1.434(7)	6.751(1)	0.676	0.000	0.025
3	0	4.742	3.7404	1.127	1.476(7)	7.653(1)	0.662	-	0.020
	2.011(9)	4.581	3.7423	1.202	1.617(7)	1.066(2)	0.394	-	0.018
4	3.752(9)	4.479	3.7400	1.273	1.756(7)	1.766(2)	0.070	-	0.021
	6.868(9)	4.145	3.7322	1.540	1.844(7)	5.143(2)	0.000	-	0.029
6	8.065(9)	3.976	3.7163	1.791	1.932(7)	2.408(3)	-	-	0.069
	8.319(9)	4.037	3.6981	1.893	2.233(7)	7.738(3)	-	-	0.163

It is now possible to compare the predicted luminosities with the results of the computations for stars of the same mass. Table 4 lists the difference in bolometric magnitude for stars of 1.25 $M_\odot$ relative to Model *B* both from the evolutionary tracks at the C^{12} burning phase, and from equation (2). The relative luminosities of the computed models on their approach to the main sequence follow closely the luminosity expected using crude relations.

TABLE 4

Comparison of the Computed and Predicted Mean Magnitudes on the Pre-Main Sequence C^{12} Burning Core (Points 0 to 2)

Model	*Evolutionary Models*	ΔM_{bol} $-2.5 \log \frac{\mu^{7.22}}{[Z(1+X)]^{1.02}(XZ)^{0.02}}$
B	0	0
F	−0.38	−0.46
H	−0.92	−1.15
I	+0.54	+0.58

V. Central Hydrogen Burning

The main sequence and post-main sequence evolutionary tracks on the (log T_e, M_{bol}) plane are shown in Figure 2 for Models *A*, *B*, *C* and *D* ($X = 0.60$, $Z = 0.10$). In Figure 2 and Table 3, points

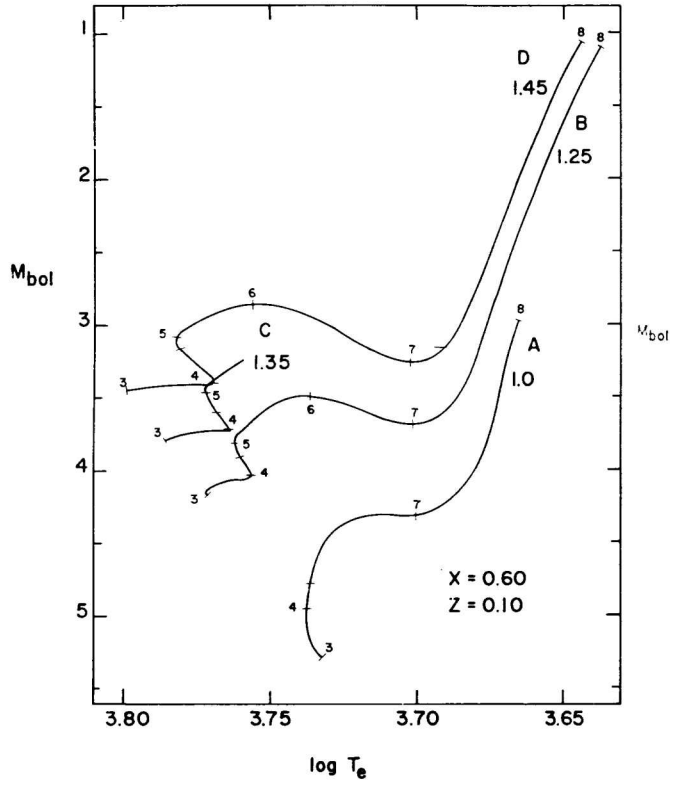

Fig. 2.—*Main sequence and post-main sequence evolutionary tracks of Models of Z = 0.10, X = 0.60. Central hydrogen burning takes place from points 3 to 4; rapid contraction and shell development from points 4 to 5; thick shell burning phase, from points 5 to 6; shell narrowing phase, from points 6 to 7; and, post-main sequence Hayashi tracks occur beyond point 7.*

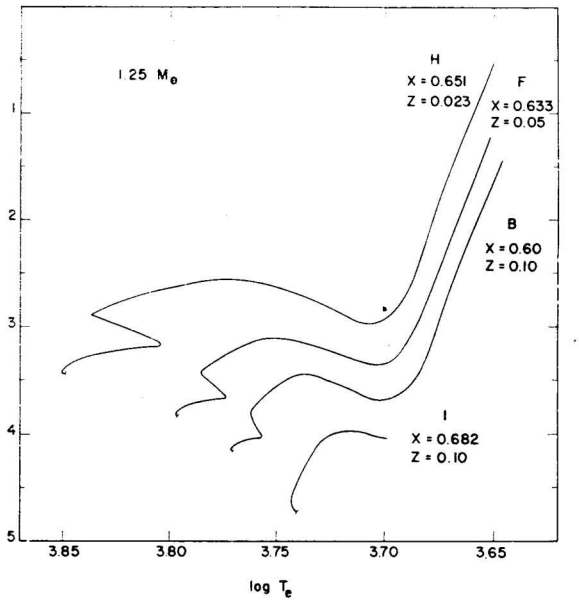

Fig. 3.—*Evolutionary paths of stars of 1.25* $M_\odot$ *of different chemical composition. Shown are Models* H, F, B, *and* I, *in order of decreasing luminosity.*

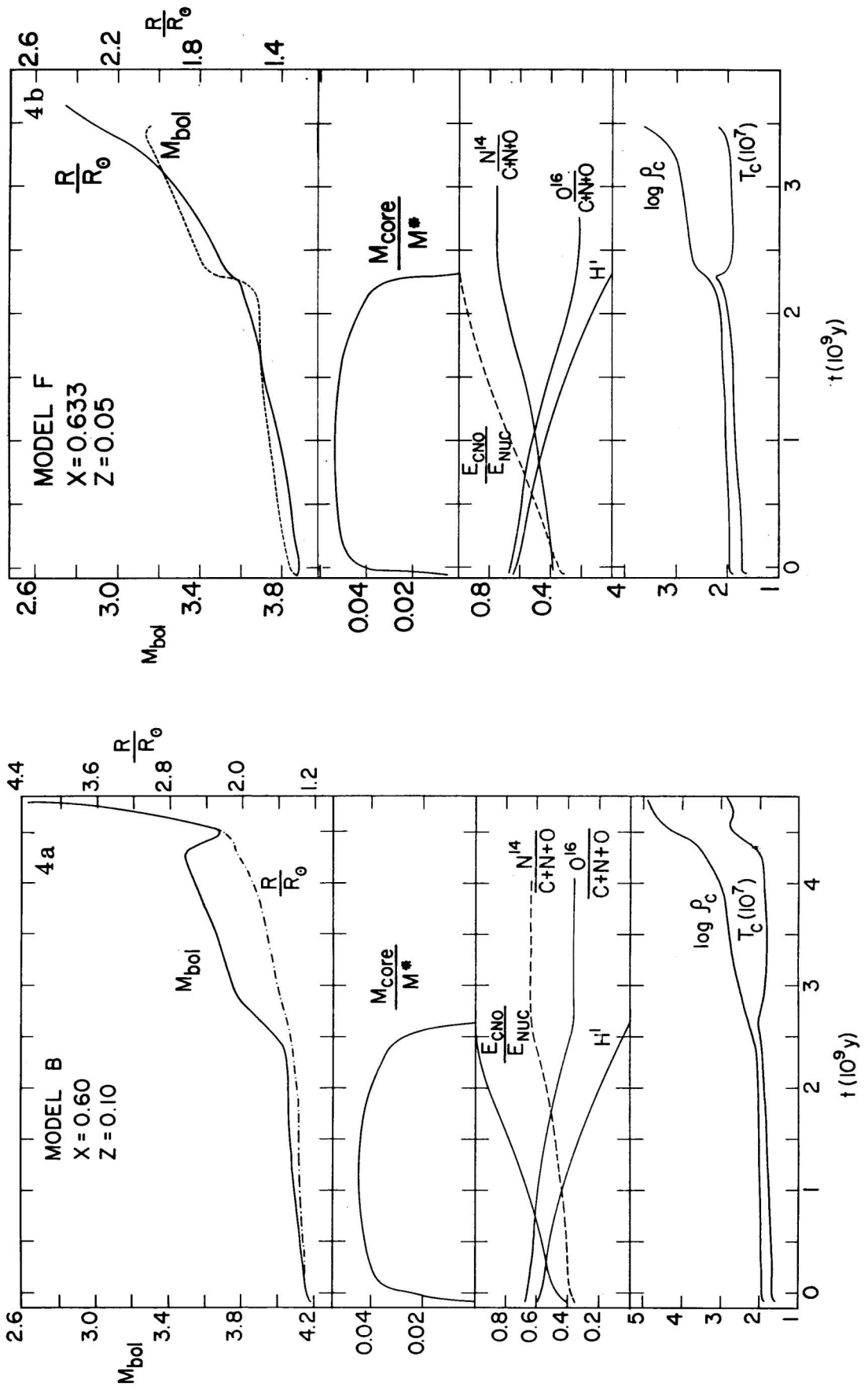

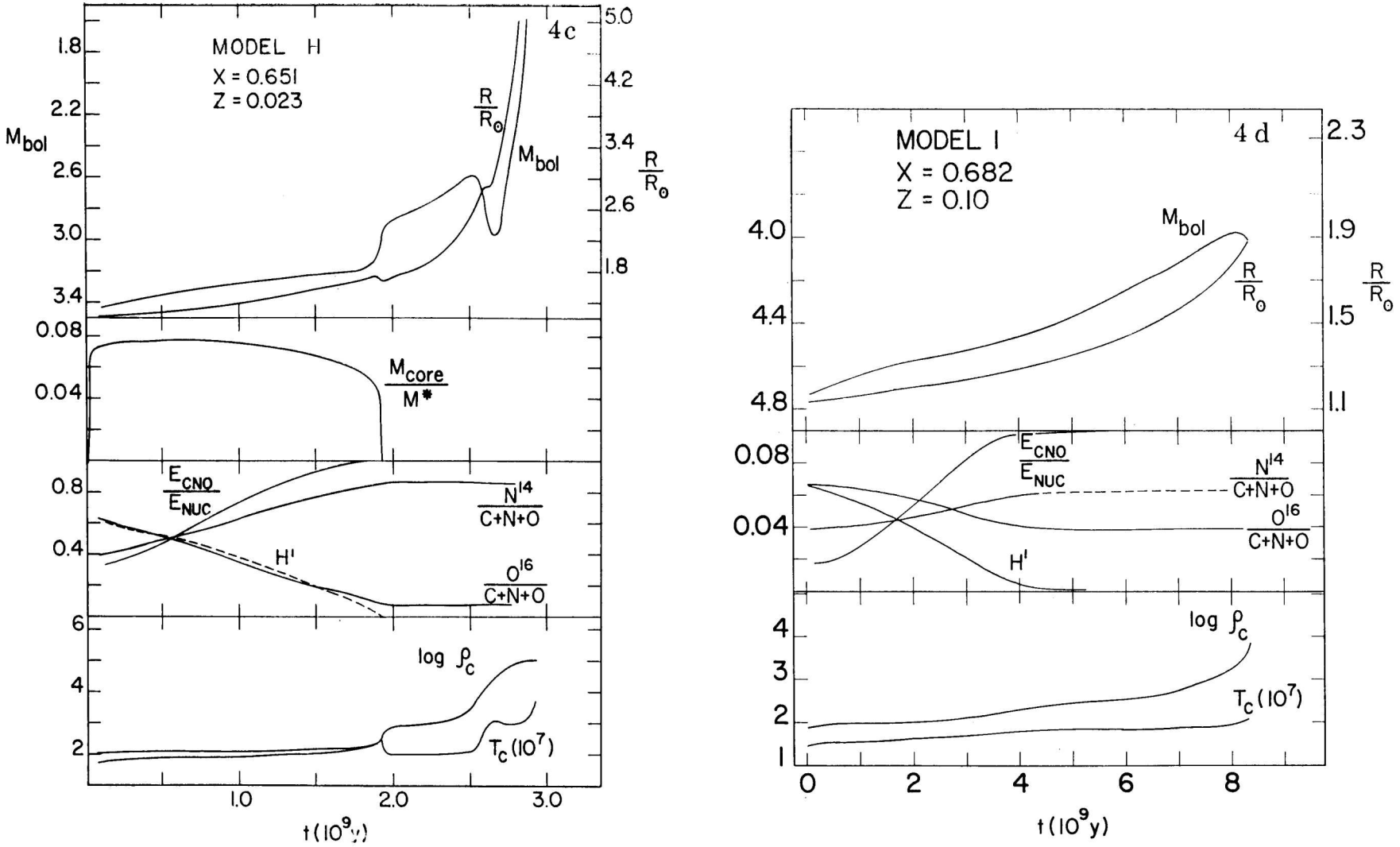

Fig. 4.—*The time dependence of surface characteristics for main sequence and post-main sequence evolution for Models of 1.25 $M_\odot$. The top section exhibits the total radius, and bolometric magnitude; the second section displays the mass fraction of the convective core; the third section exhibits the central behavior of mass ratio of N^{14} and O^{16} to total CNO elements, the mass fraction of hydrogen, and the ratio of the energy generation per gram due to the CNO cycle to the total energy generation coefficient; the bottom section depicts central temperature and density.*

marked by 3 represent the beginning of the main sequence. Point 4 marks the minimum effective temperature that the more luminous evolutionary configurations undergo just prior to complete exhaustion of the central hydrogen; these local minima of surface temperature appear in those sequences that have a convective core during the main sequence; for the configurations that do not possess a convective core, their tracks on the H-R diagram do not exhibit these minima of effective temperature, and point 4 refers to the time when only 0.07 by mass of hydrogen is left in the center. Point 5 refers to the local maximum of the effective temperature soon after the convective core has disappeared; for the sequences that do not have a main sequence convective core, no point 5 is assigned. The unmarked slash intermediate between point 4 and 5 indicates the disappearance of the convective core. Points 6 represent the maximum luminosity reached during thick shell burning; for those configurations that do not exhibit such local maximum, no point is marked. Minimum luminosity at the base of the red giant branch is indicated by point 7. For those evolutionary models that were continued to the red giant phase, point 8 marks the most advanced stages computed.

The shape of the evolutionary tracks on the H-R diagram of the computed models depends mainly on the luminosity (or mass, for a given composition). On the early stages of the main sequence the luminosity increases for all the models, while the change in surface temperature of the configurations gradually shifts from a redward displacement to a blueward displacement as stellar mass is decreased (points 3 to 4). The sharp turn to higher temperatures at the time of central hydrogen exhaustion (points 4 to 5) becomes less pronounced with decreasing mass until it finally disappears for luminosities fainter than 4.2 mag, since this effect is directly related to the size of the convective core in the main sequence stage. The total rise in luminosity through the main sequence and thick shell hydrogen burning phase (points 3 to 6) increases with decreasing mass. The evolutionary tracks on the H-R diagram for objects of the same mass, 1.25 $M_\odot$, and different composition is shown in Figure 3. From this figure it can be seen that the difference on the evolutionary tracks listed above are *basically dependent on the main sequence luminosity,* although for a given chemical composition these variations would appear to be mass-dependent.

In order to study the differences with chemical composition of the evolution of stars of the same mass, the time behavior of central and surface characteristics for models of 1.25 $M_\odot$ has been plotted and appears in Figure 4 for Models *B, F, H,* and *I.* For all the four models displayed luminosity and radius increase monotonically during the main sequence. Central density and temperature also increase throughout central hydrogen burning. In the central region hydrogen is depleted both by the p-p chain and the CNO cycle at the same time. In the four cases considered, the central temperature is high enough to deplete the original O^{16} nuclei through the link $O^{16}(p, \gamma)\ F^{17}(e^+ \nu)\ O^{17}(p, \alpha)\ N^{14}$. Since the more luminous models have higher central temperatures, the initial O^{16} abundances become reduced to 0.59, 0.55, 0.34, and 0.15 of the original value for models *I, B, F,* and *H,* respectively.

For the models examined, O^{16} and N^{14} do not reach equilibrium because the mean lifetime for the reaction $O^{16}(p, \gamma)\ F^{17}$ is similar to the time spent on the main sequence. From the tabulation by Caughlan and Fowler (1962) an approximate expression can be written for the mean lifetime of the $O^{16}(p, \gamma)\ F^{17}$ reaction

$$\log \tau = 18.5 - 0.434 T_6 - \log (\varrho X) , \qquad (3)$$

valid for the range $15 \leq T_6 \leq 25$, where τ is given in years, and X is hydrogen content by mass. Using this expression for Model *B,* the mean lifetime of central O^{16} is 3×10^9 years at the beginning of the main sequence and at the epoch the hydrogen left is 0.10 by mass, the lifetime is of 7×10^8 years, a value still too large for this nucleus to achieve equilibrium with N^{14}.

Due to the continuous increase in temperature and decrease in hydrogen abundance, the fraction of energy produced by the CNO cycle at the center of the star increases monotonically until it becomes practically the only source of energy just prior to hydrogen exhaustion (see Figure 4).

The presence of a hydrogen burning convective core for all the models computed appears to be determined mainly by the luminosity of the models. For the compositions under study, no core was present for an age zero main sequence fainter than $M_{bol} = 4.6$. Since the range of hydrogen abundance used in the present study (0.68 to 0.60) is too limited to yield any significant data on the dependence with hydrogen abundance, there is no contradiction with the investigation by Demarque (1968), who found that the minimum luminosity for a convective core does not vary significantly with metal abundance, but that this minimum luminosity can be lowered by approximately 1.0 mag when the hydrogen abundance is varied from 0.67 to 0.37 by mass. For models of the same mass, the size of the convective core is larger for the more luminous configurations. Model *I* does not have a convective core, while the cores for Models *B, F,* and *H* at maximum size are 0.045, 0.054, and 0.078 of the total mass, respectively.

Figure 4 shows that the values of the central density and temperature are higher for the more luminous models of the same mass at similar stages of evolution, and throughout the main sequence, the fractional variations of central temperature and density are more extreme for the more luminous models.

The evolutionary time scale is shorter for the more luminous configurations of the same mass, since the time that a star spends on the main sequence is proportional to its hydrogen content, and inversely proportional to the total luminosity, $\tau \propto X/L$.

Using equation (1) for the p-p cycle, $\varepsilon_0 \propto X^2$, at $T \sim 2 \times 10^7$°K, $\nu = 3.5$; and bound-free opacity $\kappa_0 \propto Z(1 + X)$, the main sequence lifetime is proportional to

$$\tau \propto \frac{X^{1.16}[Z(1+X)]^{1.08}}{\mu^{7.83}} . \qquad (4)$$

A comparison of the lifetimes of the 1.25 $M_\odot$ configurations relative to Model *B* is given in Table 5, where the first column lists the values from the evolutionary computations taken from Table 3, and the second column lists those obtained from equation (4). These two columns differ significantly, but taking into account the relative sizes of the convective core, the third column is obtained, which follows closely the computational results.

Table 6 shows the relative lifetimes of the configurations of 1.25 $M_\odot$ for the different stages of evolution. Since the evolution of Models *F* and *I* was not continued to the base of the red giant branch, the relative times are referred to the total time needed to reach the local maximum in luminosity at the time of hydrogen shell burning (point 6). For Models *B* and *H* that were evolved

TABLE 5

Main Sequence Lifetimes from Evolutionary Computations and a Simple Analytic Approximation

Model	*Evolutionary Computations*	τ*	τf†
B	1.0	1.0	1.0
F	0.896	0.679	0.81
H	0.750	0.359	0.62
I	1.55	2.01	—

* Given by equation (4).
† f is the fractional mass of the convective core.

TABLE 6

Relative Lifetimes

Phase Description	*Lifetime Percentages*			
	Model I	*Model B*	*Model F*	*Model H*
Pre-Main Sequence 0 – 3	2.9	3.2	1.8	1.0
Hydrogen Burning in the Center 3 – 4	45.1	54.9	62.6	71.7
Rapid Contraction Plus Shell Development 4 – 5	—	8.3	5.9	4.3
Hydrogen Burning in a Thick Shell 5 – 6	51.9	33.6	29.7	23.0

further, the time to reach the local maximum in luminosity (point 6) was 95% of the time to reach the base of the red giant branch, and therefore it is believed that relative times are well represented in Table 6.

In Figure 5 the radial position of internal mass points has been plotted as function of time for the four computed models of 1.25 $M_\odot$. On these "flow diagrams" the numbers on each line refer to the fractional mass. The boundary of the core has also been indicated on the figures. The dotted lines marked $E_{\max}$ correspond to the maximum of the energy generation per gram and the unmarked dashed lines refer to the position where energy generation is 1% of maximum at a given time. During

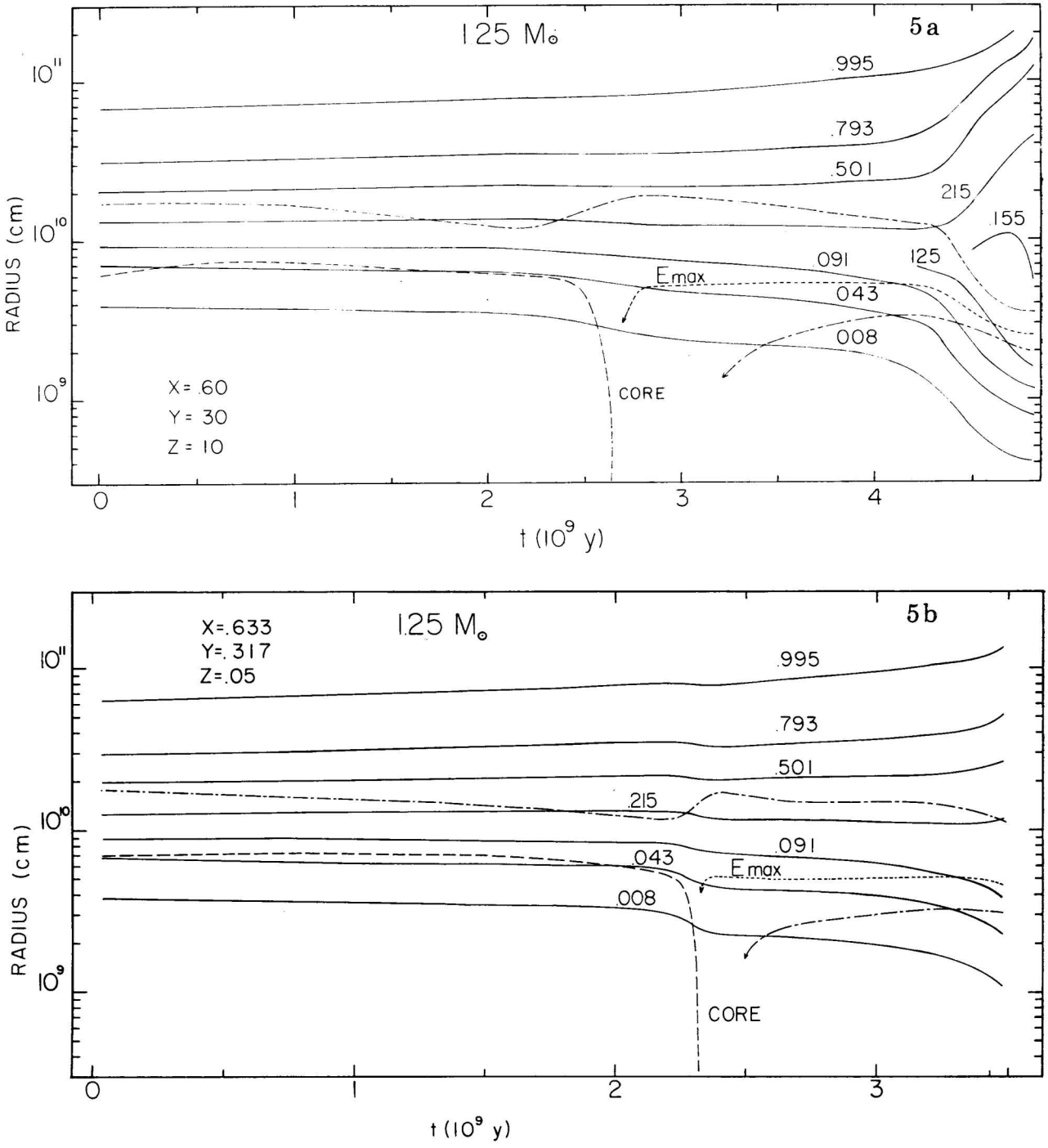

Fig. 5.—*Time variation of the radial distances of internal mass points points of Models B and F (Figures 5a and 5b, respectively). On each curve the corresponding mass fraction is indicated. Also included are the core boundary, the maximum of the energy generation per gram,* E_{max}, *and the position of the regions where energy generation is* $E_{max}/100$ *(unmarked dashed lines).*

the early main sequence the convective core develops rapidly to its maximum size and slowly recedes, leaving a small region of partially consumed hydrogen. For all the four models displayed during central hydrogen burning there is a gradual contraction of the inner regions at the same time that the outer regions expand throughout the main sequence; the configurations are divided into two zones, a contracting nuclear energy producing region and an expanding inert outer region.

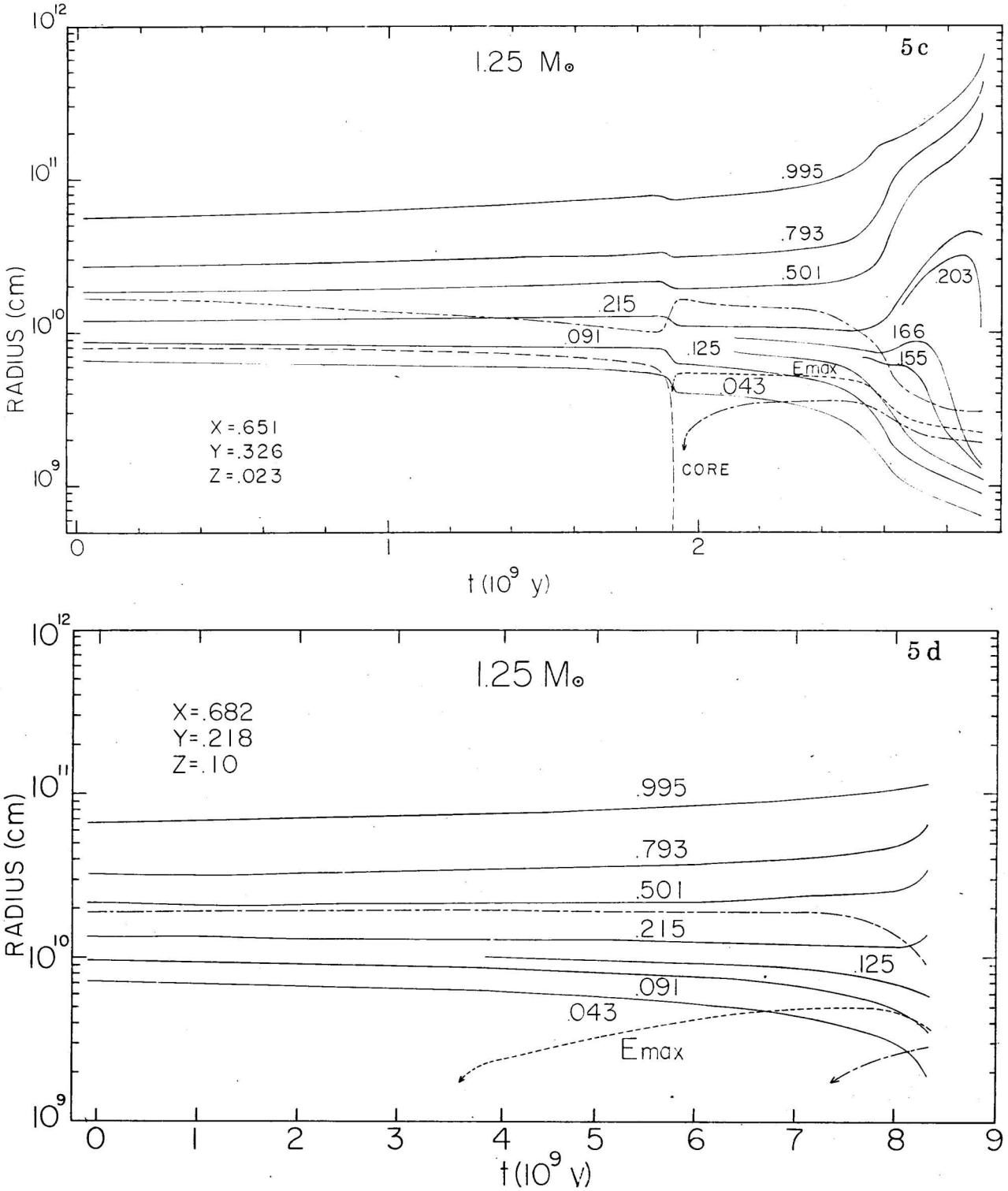

Fig. 5.—*Time variation of the radial distances of internal mass points of Models H and I (Figures 5c and 5d, respectively). Indicated are the core boundary, the maximum of the energy generation per gram,* E_{max}, *and the position of the regions where energy generation is* $E_{max}/100$ *(unmarked dashed lines).*

VI. Central Hydrogen Exhaustion Phase

The behavior of models that do not have a convective core during the main sequence does not change substantially when central hydrogen is depleted and the transition to a hydrogen burning shell takes place. In the main sequence stage hydrogen burning occurs for these configurations over a very extended zone, being more intense at the center; but even before central hydrogen is exhausted, the maximum rate of energy generation per gram already takes place in a shell and not in the center, (see Figures 4*d* and 5*d*). Therefore, at the time of central hydrogen exhaustion the inner regions continue contracting; causing the central temperature and density to increase as well as the total luminosity, while the outer zones expand and the total radius increases at essentially the same rate as before (Figure 5*d*). That is, on the H-R diagram there is no discontinuity or fast traversal.

Alternatively, a series of rapid phenomena occur just prior to complete central hydrogen exhaustion for stars with a hydrogen burning convective core. During the central hydrogen burning phase the core contains essentially the same mass, although the energy-producing region becomes more concentrated toward the center (Figs. 5*a* to 5*c*). At the time that central hydrogen has been depleted to a value that ranges from 0.05 to 0.11 by mass for our models, the nuclear energy from the core is insufficient to support the star, the inner regions of the configuration undergo rapid contraction causing central temperature and density to rise accordingly (Figs. 4*a* to 4*c*). Due to the increase in central temperature the luminosity increases abruptly while the total radius remains practically constant, causing the evolutionary track on the H-R diagram to bend toward more luminous and bluer regions. The inner regions contract at an increased rate, thereby including more mass in the nuclear energy production, and when the central hydrogen has been totally depleted, the core disappears and a hydrogen burning shell source takes over the production of energy of the whole configuration. Once the convective core has disappeared, the hydrogen depleted material continues to contract, increasing the central density, while the central temperature decreases until it reaches radiative equilibrium with the rest of the inert core. The time spent on this sharp turn on the H-R diagram is much shorter than the time spent on the main sequence; this contraction takes place on a Kelvin time scale. The relative lifetimes of contraction and shell development phases (points 4 to 5) are listed in Table 6.

Upon the disappearance of the convective core, the energy is generated over a wide region around the center, rapid contraction stops and evolution proceeds within a well defined hydrogen shell (point 5). Evolution now continues on a nuclear time scale. The rate of the luminosity increase diminishes and the track on the (log T_e, M_{bol}) plane resumes toward more luminous and redder regions.

For the configurations with convective core during the main sequence, the increase in luminosity and effective temperature is larger for more luminous models and the slope of the track on the H-R diagram is flatter. The increase of the central density is also more extreme for the brighter configurations.

In the case of Model *B*, contraction during central hydrogen exhaustion occurs only for the inner regions while the external regions continue expanding, in the case of Model *H* (Figures 5*a* and 5*c*), *all* the layers of the star undergo rapid contraction and when the core disappears the inner layers continue to contract, while the outer layers are no longer falling in.

The brighter configurations of the same mass spend a smaller fraction of their lives on the phase of contraction at the end of central hydrogen burning, as can be derived from Table 6.

VII. Post-Main Sequence Evolutionary Phases

Only those stages of the configurations characterized by the presence of a hydrogen burning shell surrounding the inert core will be described here, without reaching the phase of helium burning When central hydrogen becomes exhausted, a very wide hydrogen burning shell takes over the energy production of the star; this shell includes material already partially depleted of its original hydrogen. All the models are divided into two zones, the inner contracting layers and the outer expanding layers (see Figure 5); the contracting layers include not only the inert core, but also most of the hydrogen burning shell; while the expanding layers contain the external part of the nuclear burning region and all the material up to the surface. The contraction of the inner zone heats up the energy producing region increasing the rate of nuclear reactions and increasing the pressure on the outer strata of the shell, causing the expansion of these layers; that is, the hydrogen burning shell decreases in mass at the outer boundary. Furthermore, when the inner boundary of the shell has transformed all its hydrogen into helium, it becomes a part of the inert core and continues contracting. Both processes gradually reduce the mass that comprises the hydrogen burning shell.

The peak of the energy generation moves outward in mass, although it remains practically at constant radius, thus the hydrogen-rich material is actually falling in through the shell. The phase

of thick shell burning can be identified on the H-R diagram from the point where slow evolution proceeds redward until the maximum in luminosity is reached at intermediate temperatures before the red giant phase (points 5 to 6). The time spent on the thick shell burning phase, τ_{sh}, depends on the difference between the mass of the Schönberg-Chandrasekhar limit and the mass of the main sequence hydrogen depleted core. Thus the relative lifetime, τ_{sh}/τ_{ms}, decreases with luminosity for stars of the same mass, as can be obtained from Table 6.

The evolutionary tracks continue monotonically toward lower temperatures; the luminosity initially decreases, until it reaches a minimum (point 7) at an effective temperature of approximately 5 000°K, and thereafter increases very rapidly by several magnitudes. The initial decrease in luminosity (points 6 to 7) is due to the combined effect of the rapid expansion of the outer layers of the star and to the decrease in size of the nuclear energy producing shell.

The reduction in luminosity is smaller for fainter evolutionary sequences, and in general, for models of the same mass it decreases with luminosity. During this phase of evolution, contraction of the core proceeds at a faster rate due to the increased rate of heat diffusion as the depleted core is compressed by the pressure exerted by the outer layers of the star (Henyey and Ulrich 1972). During the shell narrowing phase a large temperature gradient is built up between the center and the shell, the heat being supplied by the release of gravitational energy. During this phase, not only the mass of the shell source decreases, but the radius of the peak of the generation of energy decreases with time.

The minima of luminosity at the bottom of the red giant branch, point 7, occur at higher effective temperatures for the brighter main sequence configurations of the same mass, since the post-main sequence Hayashi tracks for the less opaque configurations fall at higher effective temperature.

The increase in luminosity beyond points 7 occurs when photospheric layers outside the growing convective envelope begin to significantly influence energy production in the shell. As the stellar radius increases and the effective temperature decreases, the outer convective zone grows. Since the star cannot move into its own forbidden region in the H-R diagram, it evolves nearly along the boundary of this region with increasing luminosity. In these stages of evolution the stellar radius is determined by the surface condition, that is, it is adjusted by the extent of the outer convective zone almost independently of the structure of the inner region, while the luminosity is determined by the mass of the core, almost independently of the surface condition and even of the stellar total mass.

The hydrogen burning shell continues to decrease in thickness beyond point 7. Core temperatures and densities continue to rise rapidly until electron degeneracy begins to assume a dominant role in supplying core pressure, causing a drop in central temperature.

During the post-main sequence Hayashi track the peak of hydrogen burning takes place at smaller radius, but the shell eventually stops losing mass from the outer boundary. As the peak advances in mass, material that had already been part of the shell falls into it again, causing the expanding outer zone to reduce its mass —since some of the layers expanding until then are reversing their motion and falling back into the nuclear energy producing regions (see Figures 5*a* and 5*c*).

As the core becomes more degenerate, electron conduction becomes more effective. The central temperature drops until it approaches shell temperatures. The net result is a second approach to isothermal conditions within the hydrogen exhausted core.

In the meantime, the surface layers offer some interesting features. During the red giant phase the effective temperature decreases causing the extent of the convective envelope to increase until it reaches the hydrogen burning shell. At this point the shell requires additional hydrogen rich material and the envelope is pushed out by the shell. The net effect is that the convective envelope includes regions that had already undergone partial burning and thus bring up to the surface this material. Therefore, there is a change in the chemical abundance of the observable matter. The N^{14}/C^{12}, N^{14}/O^{16} and C^{13}/C^{12} abundances increase until the time of maximum size of the envelope; at later stages the surface chemical composition is no longer changed. These chemical variations have been studied in detail (Torres-Peimbert and Peimbert 1971) and have been compared to observations of planetary nebulae.

VIII. Conclusions

We present detailed computations of evolutionary tracks of models with high Z that are suitable for comparison with observations of different objects, like H-R diagrams of galactic clusters and individual stars, as well as chemical abundances from planetary nebulae. Some features of the evolutionary sequences can be predicted from our computations and are summarized below.

The slope of the age zero main sequence varies with chemical composition in the mass range computed. The main sequence is steeper for the higher Z configurations, this effect is not present in

the computations by Demarque and Schlesinger (1969) where main sequences of widely different compositions are parallel to each other.

For the range of compositions under discussion the presence of a main sequence convective core depends on the luminosity of the star. Only configurations with an age zero main sequence brighter than 4.6 mag. had a core; and the maximum central hydrogen burning lifetime for models with a core was 4.2×10^9 years. Thus, according to these models the presence of a gap in the observed H-R diagram of a cluster does not imply high metallicity (since there were cores present for $X = 0.651$, $Z = 0.023$) but it necessarily implies ages lower than 4.2×10^9 years.

From the models reported here the loci of points of the same age has been determined by Torres-Peimbert (1969, 1971) and have been compared to the H-R diagram of SMR clusters: in the case of NGC 188 an age of 3.6×10^9 years was found for $Z = 0.06$ and for NGC 6791 an age of 4×10^9 years was derived for $Z = 0.10$. For the nucleus of M31 Spinrad and Taylor (1971*b*) have obtained the main sequence turnoff point to be at G0V; from comparison with our models and those of Aizenman, Demarque, and Miller (1969) Spinrad and Taylor have established that star formation in a large scale ceased from 2 to 3×10^9 years ago. These models have also been the basis for the age determinations of individual SMR field stars by Torres-Peimbert and Spinrad (1971), who found that the SMR field K-giants are of intermediate age, *i. e.*, of about $5\text{-}6 \times 10^9$ years old.

The late L. G. Henyey gave invaluable advice and made possible the development of this work; to him I am very grateful. I thank H. Spinrad and M. Peimbert for helpful discussions; A. N. Cox and D. D. Eilers for computing opacity tables of very high Z; W. B. Hubbard for supplying the program to compute conductive opacities; J. E. Forbes and E. Simpson for their great assistance with the stellar evolution program.

REFERENCES

Aizenman, M. L., Demarque, P., and Miller, R. H. 1969, *Ap. J.*, **155**, 973.
Aller, L. H. 1961, *The Abundances of the Elements* (New York: Interscience Publishers), p. 115.
Bergh, S. van den and Sackman, I. J. 1965, *A. J.*, **70**, 353.
Bodenheimer, P., Forbes, J. E., Gould, N. L., and Henyey, L. G. 1965, *Ap. J.*, **141**, 1019.
Caughlan, G. R., and Fowler, W. A. 1962, *Ap. J.*, **136**, 453.
Cox, A. N. 1965, *Stellar Structure, Vol. 8: Stars and Stellar Systems*, ed. L. Aller and D. McLaughlin (Chicago: Univ. of Chicago Press), p. 195.
Cox, A. N. and Stewart, J. N. 1965, *Ap. J. Suppl.*, **11**, 22.
———. 1968, (private communication).
———. 1970, *Ap. J. Suppl.*, **19**, 243.
Cox, A. N., Stewart, J. N., and Eilers, D. D. 1965, *Ap. J. Suppl*, **11**, 1.
Demarque, P. 1968, *Ap. J.*, **73**, 669.
Demarque, P., and Heasley, J. N., Jr., 1971, *Ap. J.*, **163**, 547.
Demarque, P. and Larson, R. B. 1964, *Ap. J.*, **140**, 544.
Demarque, P. and Schlesinger, B. M. 1969, *Ap. J.*, **155**, 965.
Goldberg, L., Müller, E. A., and Aller, L. H. 1960. *Ap. J. Suppl.*, **5**, 1.
Greenstein, J. L. and Oinas, V. 1968, *Ap. J. (Letters)*, **153**, L91.
Henyey, L. G., Forbes, J. E., and Gould, N. L. 1964, *Ap. J.*, **139**, 306.
Henyey, L. G., and Ulrich, R. K. 1972, (in press).
Henyey, L. G., Vardya, M. S., and Bodenheimer, P. 1965, *Ap. J.*, **142**, 841.
Hubbard, W. B. and Lampe, M. 1969, *Ap. J. Suppl.*, **18**, 297.
Iben, I., Jr. 1963, *Ap. J.*, **138**, 452.
Krishna Swamy, K. S. 1966, *Ap. J.*, **145**, 174.
———. 1968, *P. A. S. P.*, **80**, 406.
Pagel, B. E. J. 1966, *Abundance Determinations in Stellar Spectra, I. A. U. Symposium No. 26*, ed. H. Hubenet (London: Academic Press), p. 359.
Pearce, W. P. and Bahng, J. 1965, *Ap. J.*, **142**, 164.
Reeves, H. 1965, *Stellar Structure, Vol. 8: Stars and Stellar Sytems*, ed. L. H. Aller and D. McLaughlin (Chicago: Univ. of Chicago Press), p. 113.
Schwarzschild, M. 1958, *Structure and Evolution of the Stars*, (Princeton, N. J.: Princeton Univ. Press), p. 103.
Spinrad, H., Greenstein, J. C., Taylor, B. J., and King I. R. 1970, *Ap. J.*, **162**, 891.
Spinrad, H. and Luebke, W. R., Jr. 1970, *Ap. J.*, **160**, 1141.
Spinrad, H. and Peimbert, M., 1972, *Stars and Stellar Systems, Vol. 9: Galaxies and the Universe*, ed. A. Sandage and M. Sandage (Chicago: University of Chicago Press), (to be published).
Spinrad, H. and Taylor, B. J. 1967, *A. J.*, **72**, 320.
———. 1969, *ibid.*, **157**, 1279.
———. 1971*a*, *ibid.*, **163**, 303.
———. 1971*b*, *Ap. J. Suppl.*, **22**, 445.
Taylor, B. J. 1967, *P. A. S. P.*, **79**, 441.
———. 1970, *Ap. J. Suppl.*, **22**, 177.
Torres-Peimbert, S. 1969, University of California, Berkeley, Thesis.
———. 1971, *Bol. Obs. Tonantzintla y Tacubaya*, **6**, 3.
Torres-Peimbert, S. and Peimbert, M. 1971, *Bol. Obs. Tonantzintla y Tacubaya*, **6**, 101.
Torres-Peimbert, S. and Spinrad H. 1971, *Bol. Obs. Tonantzintla y Tacubaya*, **6**, 15.
Upton, E. K. J., Little, S. J. and Dworetsky, M. M. 1968, *Ap. J.*, **154**, 597.
Watson, W. D. 1970, *Ap. J. Suppl.*, **19**, 235.